Journal of Physics and Chemistry of Solids 86 (2015) 170–176

Contents lists available at ScienceDirect

Journal of Physics and Chemistry of Solids

journal homepage: www.elsevier.com/locate/jpcs

Synthesis, photoluminescence and thermoluminescence properties of $LiNa_3P_2O_7:Tb^{3+}$ green emitting phosphor

K. Munirathnam [a,d], G.R. Dillip [b,*], B. Ramesh [a], S.W. Joo [b,*], B. Deva Prasad Raju [a,c,*]

[a] Department of Physics, Sri Venkateswara University, Tirupati 517502, India
[b] School of Mechanical Engineering and Technology, Yeungnam University, Gyeongsan 712-749, South Korea
[c] Department of Future Studies, Sri Venkateswara University, Tirupati 517502, India
[d] School of Physical Sciences, Reva University, Bangalore 560 064, India

ARTICLE INFO

Article history:
Received 2 June 2015
Received in revised form
10 July 2015
Accepted 14 July 2015
Available online 15 July 2015

Keywords:
Alloys
Chemical synthesis
X-ray diffraction
Microstructure
Luminescence

ABSTRACT

The alkaline phosphate based $LiNa_3P_2O_7:Tb^{3+}$ phosphors are prepared by solid state reaction method. X-ray diffraction (XRD) analysis shows that all the powders possess orthorhombic structure. Fourier transform infrared (FTIR) spectroscopy studies suggest that the phosphor belong to the diphosphate family. The morphology of the phosphors is identified by scanning electron microscopy (SEM). Upon 378 nm excitation, the $LiNa_3P_2O_7:Tb^{3+}$ phosphors shown emission bands at 482, 545, 588 and 620 nm corresponding to the transitions $^5D_4 \rightarrow {}^7F_6$, $^5D_4 \rightarrow {}^7F_5$, $^5D_4 \rightarrow {}^7F_4$ and $^5D_4 \rightarrow {}^7F_3$, respectively. The optimized concentration of Tb^{3+} in $LiNa_3P_2O_7$ phosphor is found to be 9 mol%. The concentration quenching mechanism was proved to be the exchange interaction between two nearest Tb^{3+} ions with the critical distance (R_c) of 1.18 nm. The Commission International de l'Eclairage (CIE) coordinates evidence that the phosphors emit in the green light region. Thermoluminescence properties of the prepared phosphors are studied by pre-irradiating the powders with different doses of UV irradiation. The kinetic parameters of TL glow curves are calculated using Chen's peak shape method.

1. Introduction

In recent years, white light emitting diodes (W-LEDs) have flourished due to many advantages in their characteristics of high luminous efficiency, long durability, non-environmental pollution and less maintenance over the traditional incandescent, fluorescent and high intensity discharge lamps [1–3]. The most common methods to fabricate white light emitting diodes (W-LEDs) are the combination of yellow-emitting phosphor $YAG:Ce^{3+}$ with blue emitting InGaN based chip and the mixing of red, blue and green (RGB) LEDs to get white light [4,5]. However, the obtained white light by these mechanisms have poor color rending index (CRI) and high color correlated temperature (CCT) owing to their very weak emission intensity in red spectral region and halo effect due to different characteristics of LEDs [6,7]. The possible way to obtain white light is the fabrication of phosphor-converted white LEDs by incorporating the suitable multi-colored (such as red, green and blue) phosphors on a GaN chip, which acts as excitation source near ultraviolet (350–420 nm) region [8,9].

Recently, a great attention has been received for the development of efficient thermoluminescent (TL) materials to be applied in defect studying and dosimetry, such as detection of ionizing radiation, dating in archeology, clinical and environmental applications [10,11]. Usually, thermoluminescence of material gives the crucial information about trapping parameters such as activation energy of traps, order of kinetics and thermal stability of host materials [12]. Selection of host materials plays an important role in the photo- and thermo-luminescence of phosphors. From literature survey, it has been found that the phosphate based phosphors are considered as an ideal and potential host material because of their low sintering temperature, excellent thermal and chemical stability. Specially, orthophosphate phosphors have got great applications in lighting display systems due to their excellent properties such as large band gap, high stability and luminescence property of strong emission in visible region [13,14]. In last few decades, the thermo- and photo-luminescence properties of rare-earth (RE) ions doped phosphate host matrices have been studied widely, for instance $K_4Ca(PO_4)_2$ [15], $Ca_4(PO_4)_2O$ [16], $Ca_{10}Li(PO_4)_7$ [17], $Na_2Ca_4(PO_4)_3F$ [18]. It is well recognized that RE ions act like a kind of luminescence centers in phosphor, which is further used in the field emission displays (FEDs) and plasma display panel (PDP) devices [19,20]. Among other RE ions, particularly, terbium (Tb)

* Corresponding authors at: Department of Physics, Sri Venkateswara University, Tirupati 517502, India and School of Mechanical Engineering and Technology, Yeungnam University, Gyeongsan, 712-749, South Korea.
E-mail addresses: dillip.ngr@gmail.com (G.R. Dillip), swjoo@yu.ac.kr (S.W. Joo), drdevaprasadraju@gmail.com (B.D. Prasad Raju).

http://dx.doi.org/10.1016/j.jpcs.2015.07.011
0022-3697/

doped phosphors are well efficient to emit narrow band green light, due to an effective transition through the 4f–5d and 4f–4f under near ultraviolet (NUV) excitation. Thus, Tb^{3+} ion serves as an activator in green-emitting phosphors for fabrication of white lighting emitting diodes (W-LEDs) [21]. Over the past few decades, many reports are appeared in literature on the RE ions (Tb^{3+}) -doped phosphors, for instance, $K_3R(PO_4)_2$:Tb^{3+} (R=Y and Gd) [22], LaOCl:Ln^{3+} (Ln=Eu/Sm, Tb, Tm) [23], $CaMoO_4$:Tb^{3+} [24]. The solid state reaction (SSR) method has been recognized as a well-known conventional method for the preparation of phosphors because of their ease of synthesis. This method results in uniform sized particles and higher quantum efficiency of the phosphors. Though, several phosphors have been synthesized and reported in the past several years, the range of phosphors that are suitable for W-LEDs and thermoluminescence dosimetric (TLD) applications are limited. Therefore, in the present work, we have made an attempt to synthesize a new host material, $LiNa_3P_2O_7$ doped with rare-earth ion (Tb^{3+}) by SSR method and studied their suitability for the practical applications. To the best of our knowledge, until now, no studies have been reported on the photo- and thermoluminescence properties of Tb^{3+} ion doped $LiNa_3P_2O_7$ phosphor. Moreover, the important parameters to be applied for W-LEDs and TLD phosphor such as color coordinates, kinetic parameters (like trap depth (E) and frequency factor (s)) have been calculated and reported for the first time.

2. Experimental

2.1. Synthesis

The crystalline powders of $LiNa_{3-x}P_2O_7$:xTb^{3+} (x=0, 1, 3, 5, 7, 9 and 11 mol%) were prepared via conventional solid state reaction method. The high purity (99.99%) chemicals, Li_2CO_3, Na_2CO_3, $NH_4H_2PO_4$ and Tb_4O_7 were taken as starting materials without further purification. The stoichiometric amounts of starting materials were mixed together in an agate mortar for homogeneous mixing and taken in silica crucibles. Thereafter, the mixtures were placed at constant temperature region in muffle furnace and heated gradually, from room temperature (RT) to 450 °C for ejection of CO_2 and NH_3. Finally, the samples were annealed at 540 °C for 18 h with several intermediate grindings and used for further measurements.

2.2. Characterization

The crystal structure of $LiNa_3P_2O_7$:Tb^{3+} phosphors were analyzed by X-ray diffraction (XRD) analysis using PANalytical diffractometer (Siemens, AXS D5005) with Cu-K_α radiation (λ=0.1540 nm) at a scanning step of 0.02° in the 2θ range from 10° to 50° at 40 kV and 20 mA. The infrared spectrum was recorded by the diffuse reflection technique using a Bruker IFS Equinox 55 FTIR spectrometer in the range of 4000–400 cm^{-1}. The morphology of phosphors was investigated by scanning electron microscope (SEM) (GEMINI ULTRA 55). The elemental analysis was carried out by energy dispersive spectroscopy (EDS) using an X-ray detector attached to the SEM instrument. Photoluminescence spectra were measured by using JobinVyon Fluorolog-3 fluorescence spectrophotometer equipped with Xenon lamp as the excitation source. All the measurements were recorded at RT. TL glow curves of phosphors were recorded with Nucleonix TL reader. The usual setup consisting of a small metal plate heated directly using a temperature programmer, photomultiplier tube (931B), dc amplifier and milli volt recorder. Five milligram of phosphor was heated every time at the rate of 5 °C s^{-1} in range of 50–400 °C temperature. Prior to TL measurements, the samples were exposed to UV-irradiation using an excitation wavelength of 250 nm.

3. Results and discussion

3.1. XRD analysis

The XRD patterns of $LiNa_{3-x}P_2O_7$:xTb^{3+} (x=0–9 mol%) phosphors are shown in Fig. 1. From the figure, it is noticed that the single phase samples were successfully obtained by solid-state reaction. All the diffraction peaks obtained in the phosphors were well matched with the reports, in the Inorganic Crystal Structure Database (ICSD): 424375 and also appeared in literature [25,26]. According to the reports, the $LiNa_3P_2O_7$ was crystallized in the orthorhombic space group C_{2221} with lattice parameters, a=0.54966 nm, b=0.91365 nm and c=1.22764 nm. From XRD pattern, no extra peaks were observed due to the increase of Tb^{3+} ions concentration in the host matrix. The possible reason might be that the doped Tb^{3+} ions could occupy Na^+ ions sites, since the ionic radius of Tb^{3+} (0.092 nm, coordination number (CN)=6) is smaller than that of Na^+ (0.102 nm, CN=6) and greater than Li^+ (0.076 nm, CN=6) [27,28]. In order to verify the radius percentage difference (D_r) between the doped and substituted ions in the phosphors, the following approximation was used [29,30].

$$D_r = \left[\frac{100\,[R_m(CN) - R_d(CN)]}{R_m(CN)}\right] \quad (1)$$

where CN is the coordination number, R_m and R_d are the radius of the host cation and doped ion, respectively. The D_r between the dopant Tb^{3+} ions and host cations, Li^+/Na^+ on six co-ordinated sites were found to be −21% and 9%, respectively. From the above results, it is suggested that the dopant, Tb^{3+} ions will preferentially substitute at the sodium sites in the host. Thus, the charge loss is compensated by Na^+ vacancies (V_{Na}) by the following process:

$$3Na^{3+} \rightarrow Tb^{3+} + V_{Na} \quad (2)$$

The substitution of Tb^{3+} ions in the host cation sites induce lattice expansion, resulting the shifting of XRD peaks to the lower angle side. In order to prove the lattice expansion of the phosphors as a function of Tb^{3+} ion concentration, the orthorhombic crystal structural parameters such as unit cell constants (a, b and c) and volume (V) were calculated from the crystal geometry equations

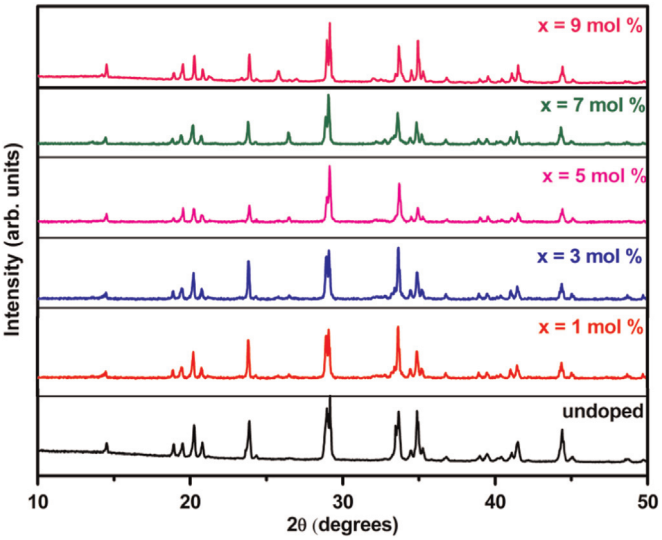

Fig. 1. XRD patterns of $LiNa_{3-x}P_2O_7$:xTb^{3+} (x=0–9 mol%) phosphors.

Table 1
Structural parameters of $LiNa_{3-x}P_2O_7:xTb^{3+}$ (x=0–9 mol%) phosphors.

Tb^{3+} concentration in $LiNa_3P_2O_7$ (mol%)	Lattice parameters			
	a (nm)	b (nm)	c (nm)	V (nm^3)
Undoped	0.5494	0.9143	1.2257	0.61573
1	0.5485	0.9133	1.2306	0.61665
3	0.5522	0.9111	1.2308	0.61933
5	0.5532	0.9099	1.2356	0.62204
7	0.5568	0.9089	1.2361	0.62567
9	0.5528	0.9087	1.2484	0.62727

using the following relations:

$$\frac{1}{d^2} = \frac{h^2}{a^2} + \frac{k^2}{b^2} + \frac{l^2}{c^2} \text{ and } V = abc \tag{3}$$

where d is the distance between adjacent planes (nm), (hkl) is the miller indices. To determine the lattice parameters, we adopted the dominant intensity lattice planes of (0 2 0), (0 2 1) and (1 3 0) for interplanar distances, d_1, d_2 and d_3, respectively. The lattice parameters of the phosphors are listed in Table 1. As shown in the table, the unit cell volume was increased as a function of Tb^{3+} ion concentration, indicating the lattice expansion in the host material.

3.2. FTIR analysis

In order to investigate the nature of chemical bonding in phosphate materials, the FTIR spectrum of $LiNa_3P_2O_7:xTb^{3+}$ (x=9 mol%) phosphor is recorded and shown in Fig. 2. According to Corbridge et al. [31], IR spectrum of pyrophosphate is divided into mainly four frequency regions, i.e., at ν_1=3654–3535 cm^{-1}, ν_2=2667.66–2337.9 cm^{-1}, ν_3=1811.79–1432.65 cm^{-1} and ν_4 =1249.65–412.58 cm^{-1} corresponding to the vibrational bands of the –OH, PO_3, PO_4 and P–O–P, respectively. From the spectrum, it is identified that there are two distinct bands near 1115 and 1017 cm^{-1}, attributed to the symmetric and asymmetric vibrational stretching modes of the PO_3 species. The band appeared at around 745 cm^{-1}, due to the symmetric stretching vibrational mode of (P–O–P) bridges in pyrophosphate (P_2O_7) group. It reveals that the material belongs to the diphosphate family [25]. Further, in the range from 600 to 400 cm^{-1}, two bands are noticed at 570 cm^{-1} and 462 cm^{-1}, owing to the vibrational modes of PO_3 groups. In addition, the spectrum consists of a very weak absorption band at 3422 cm^{-1}, indicating the presence of –OH group in the sample. This band is the characteristic vibrations of water, physically absorbed on the sample surface during the preparation time under non-vacuum condition. It is known that a minimal of –OH band decreases the optical losses thereby increasing the quantum efficiency of the phosphors [32]. However, for the present phosphors, the intensity of the IR band linked to –OH group is extremely low, may be suitable for practical applications.

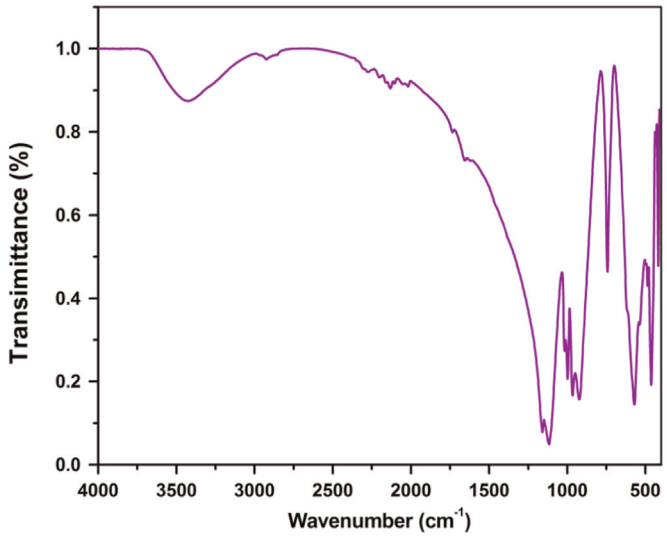

Fig. 2. FTIR spectrum of $LiNa_{3-x}P_2O_7:xTb^{3+}$ (x=9 mol%) phosphor.

3.3. Morphological and elemental analyses

In order to study the surface morphology of phosphors, SEM analysis was carried out. The SEM images of the samples, $LiNa_{3-x}P_2O_7:xTb^{3+}$ (x=5 and 9 mol%) are shown in Fig. 3(a) and (b). The morphology of samples shown agglomerated surface, it might be due to the liberation of huge amount of NH_3 and CO_2 during the synthesis. However, the approximate range of particles is in micrometer dimension, which could be suitable for white-LED application. To verify the nominal chemical composition of products, EDS spectra of samples were recorded and presented in Fig. 4(a) and (b). From the profiles, it is noticed that the compound is composed of Na, P, O and Tb elements. However, Li element was not appeared in the figures, since the used EDS could not detect the elements having atomic number below the carbon elements.

3.4. Photoluminescence studies

The typical photoluminescence excitation (PLE) spectrum of $LiNa_{3-x}P_2O_7:xTb^{3+}$ (x=9 mol%) phosphor, recorded at 545 nm emission is shown in Fig. 5. The excitation spectrum composed of several sharp bands at 308 nm ($^7F_6 \rightarrow {}^3H_6$), 319 nm ($^7F_6 \rightarrow {}^5D_0$) and 378 nm ($^7F_6 \rightarrow {}^5G_6$), respectively. These sharp bands are due to the 4f–4f transitions of Tb^{3+} [24,33]. Among the sharp lines, the broad band at about 378 nm ($^7F_6 \rightarrow {}^5G_6$) has the strongest intensity and is used further to measure the emission spectra of phosphors. From the figure, it is evidenced that the prepared sample can effectively excited at NUV wavelength. The emission spectra of $LiNa_{3-x}P_2O_7:xTb^{3+}$ (x=1–11 mol%) phosphors monitored at excitation wavelength of 378 nm are shown in Fig. 6. It can be seen that the emission spectra consist of several sharp peaks at around 482 nm, 545 nm, 588 nm and 620 nm, which are due to the transitions of $^5D_4 \rightarrow {}^7F_{J=6,5,4,3}$, respectively [23]. Among several sharp peaks, the band at 545 nm corresponds to $^5D_4 \rightarrow {}^7F_5$ transition of Tb^{3+} ions is the strongest in the $LiNa_3P_2O_7:Tb^{3+}$ phosphors. A typical energy level diagram of Tb^{3+} ions in $LiNa_3P_2O_7$ phosphor is shown in Fig. 7(a). Further, to find the effect of dopant concentration on the emission intensities of host material, the Tb^{3+} ions in host was varied. The variation of PL intensity with RE ion (Tb^{3+}) concentration is shown in Fig. 7(b). We note from the figure that the PL intensity of phosphor enhanced by increasing the dopant (Tb^{3+}) concentration from 1 to 9 mol% and thereby decreased on further increase of dopant concentration due to the concentration quenching effect. The concentration quenching phenomena will occur due to the non-radiative energy transfer between energy levels of RE ions. The critical distance (R_c) is an important parameter which determines the concentration quenching phenomena. It can be estimated according to the following formula given by Blasse and Grabmaier [34]

$$R_c = 2\left(\frac{3V}{4\pi x_c Z}\right)^{1/3} \tag{4}$$

where, V is the volume of the unit cell, x_c is the critical concentration of Tb^{3+} ions, and Z is the number of cations in the unit cell. In the current case, the values of V, x_c and Z are 0.6272 nm,

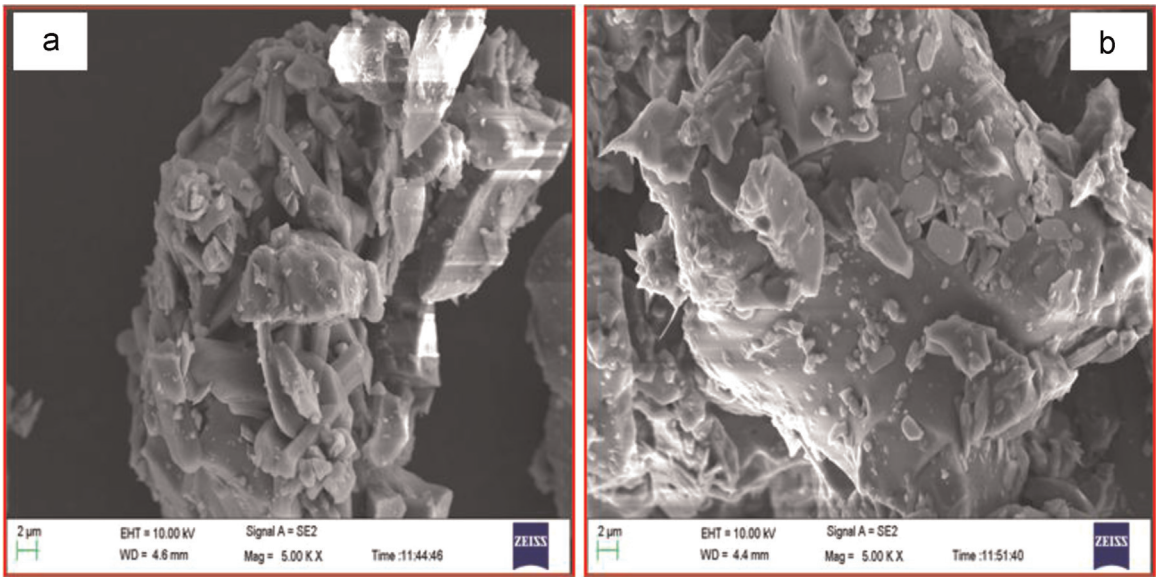

Fig. 3. SEM images of $LiNa_{3-x}P_2O_7$:xTb^{3+} phosphor, (a) $x=5$ mol% and (b) $x=9$ mol%.

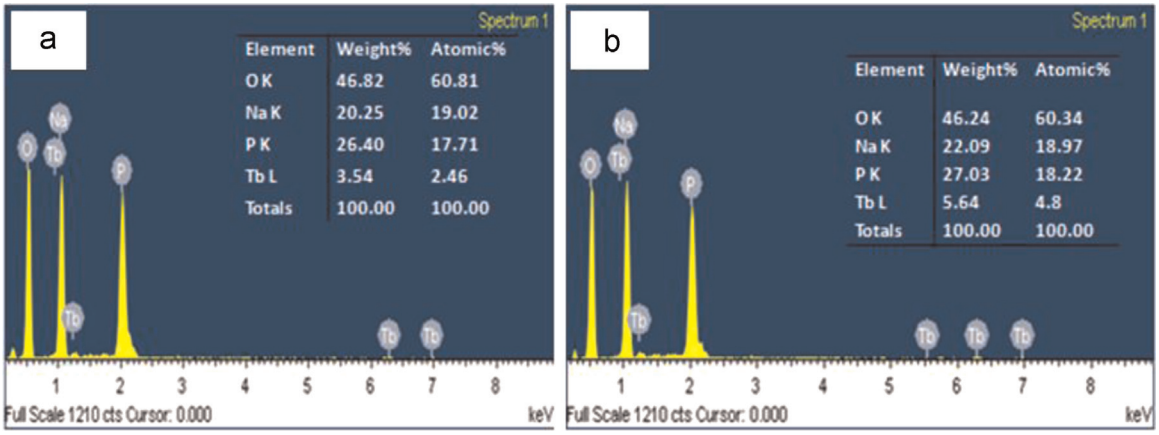

Fig. 4. EDS profiles of $LiNa_{3-x}P_2O_7$:xTb^{3+} phosphor, (a) $x=5$ mol% and (b) $x=9$ mol%.

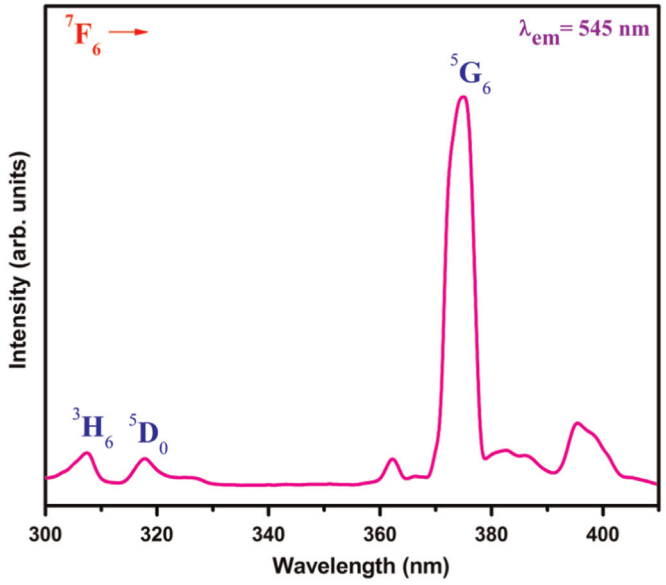

Fig. 5. Photoluminescence excitation spectrum of $LiNa_3P_2O_7$:xTb^{3+} ($x=9$ mol%) phosphor.

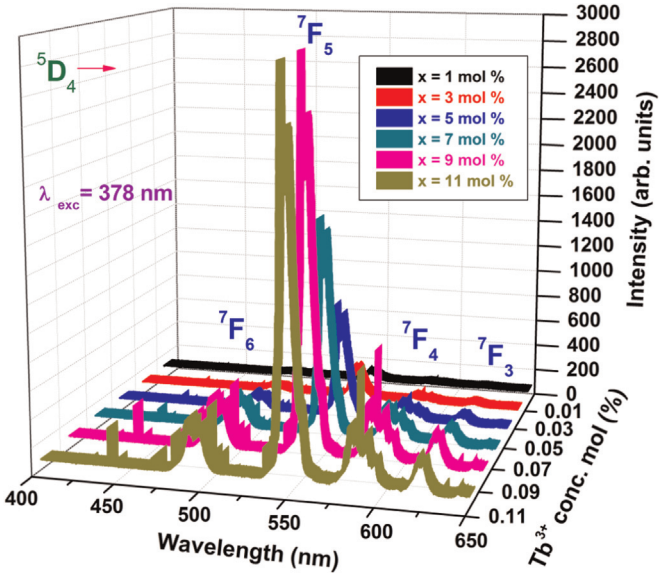

Fig. 6. Emission spectra of $LiNa_{3-x}P_2O_7$:xTb^{3+} ($x=1$–9 mol%) phosphors.

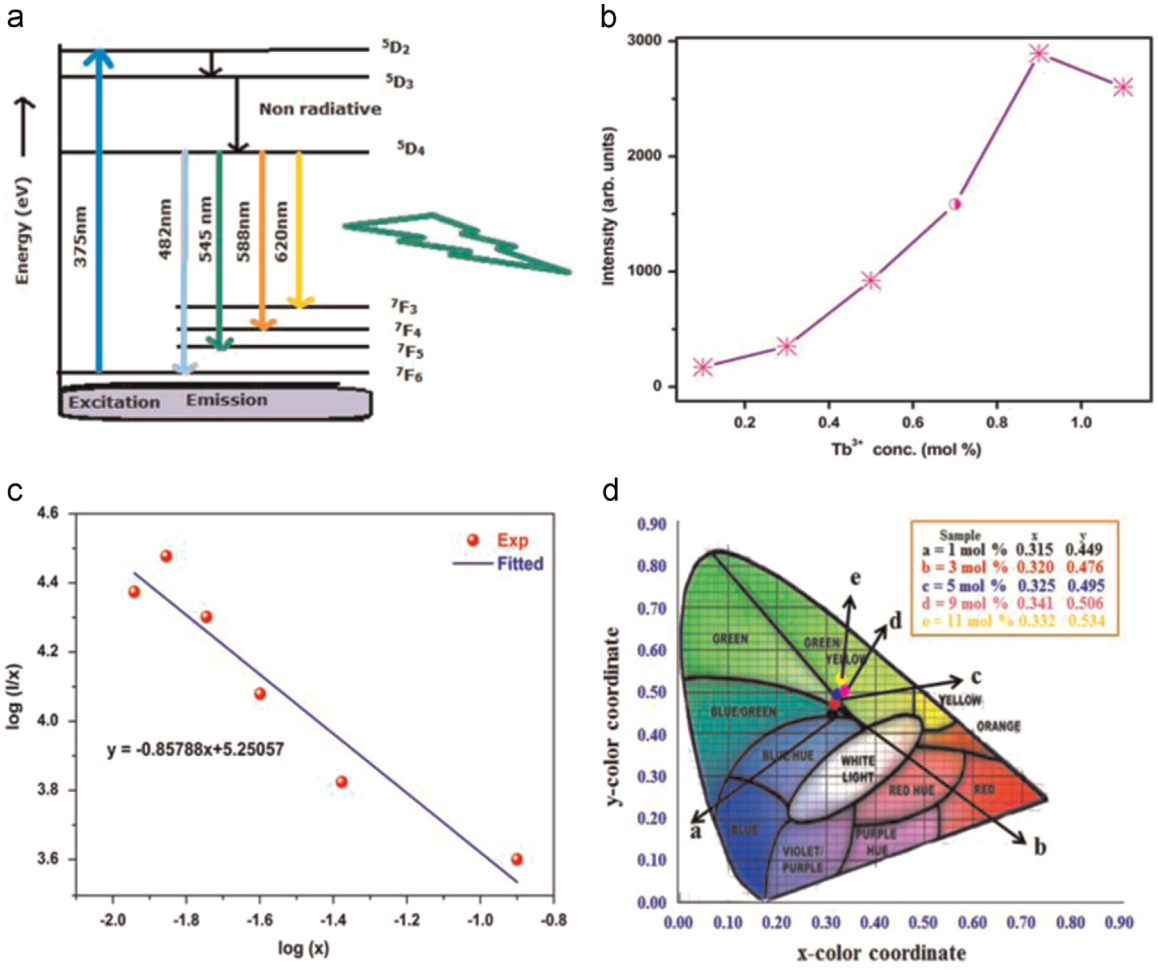

Fig. 7. (a) Schematic energy transfer mechanism of Tb^{3+} in $LiNa_3P_2O_7$, (b) Variations of emission intensity as a function of Tb^{3+} ions concentrations, (c) Plot of log (I/x) versus log (x), and (d) CIE chromaticity diagram of $LiNa_{3-x}P_2O_7$:xTb^{3+} (x=1–11 mol%) phosphors.

0.09 and 4, respectively. The R_c is found to be 1.1849 nm. According to Dexter's [35] theory, different types of energy transfer mechanism are involved in the same type of dopant ions in the host such as exchange interaction, dipole–dipole (d–d), dipole–quadrupole (d–q) and quadrupole–quadrupole (q–q) interactions. The type and strength of the interactions could be determined by VanUitert's formula from the emission spectra. The emission intensity (I) per activator ion is given by the equation:

$$\frac{I}{x} = k\left[1 + \beta(x)^{\theta/3}\right]^{-1} \quad (5)$$

where, x is the activator concentration, I/x is the emission intensity (I) per activator (x). K and β are the constants for a given host under the same excitation condition [36]. The above equation can be rearranged for $\beta(x)^{\theta/3}$»1 as follows $\log \frac{I}{x} = k' - \frac{\theta}{3}\log(x)$, where $k' = \log k - \log \beta$. The plot of log (I/x) versus log (x) is shown Fig. 7 (c). The slope ($-\theta/3$) was determined to be −0.8578. Thus, the value of θ could be calculated as 2.5734 and is approximately equal to 3. From literature reviews, θ=3 for the energy transfer among the nearest-neighboring ions, while θ=6, 8, and 10 for d–d, d–q, and q–q interactions, respectively [37]. Thus, the above results indicated that the concentration quenching mechanism of Tb^{3+} emission could be common effect of nearest-neighboring interaction in the host material. However, the emission intensity is enhanced in $LiNa_{3-x}P_2O_7$:xTb^{3+} (x=9 mol%) phosphor and evidences that the phosphor may be promising candidate for emitting green light under NUV excitation.

3.5. Chromatic properties

Commission International de l'Eclairage (CIE) color coordinates refer some specifications of light sources, which represents kind of color. In general, the color of any light source can be represented by the (x, y) coordinate in color space [38]. From the emission spectra, the CIE coordinates were calculated using the CIE calculate software under 378 nm excitation wavelength. The CIE diagram is shown in Fig. 7(d). We note from the figure that the CIE values were located in the green light region. For instance, the CIE chromaticity coordinates of $LiNa_{3-x}P_2O_7$:xTb^{3+} (x=9 mol%) phosphor is found to be (0.341, 0.506), which is in green region. Thus, the results demonstrate that the prepared phosphors may have potential application for green light emitting in the designing of W-LEDs under near UV excitation.

3.6. Thermoluminescence properties

TL properties of $LiNa_{3-x}P_2O_7$:xTb^{3+} (x=1–11 mol%) phosphors have been studied. Prior to TL measurements, the samples were subjected to the UV radiation. It was observed that the TL emission increased with dopant concentration up to 9 mol% and decreased further increase of Tb^{3+} ion concentration (not shown here). For further analysis, $LiNa_{3-x}P_2O_7$:xTb^{3+} (x=9 mol%) was exposed to UV radiation at different time intervals. The variation of TL intensity as a function of UV exposure time is shown in Fig. 8. From the glow curves, it was noticed that the shape and position of TL peaks are similar to appear for all UV exposure times. However,

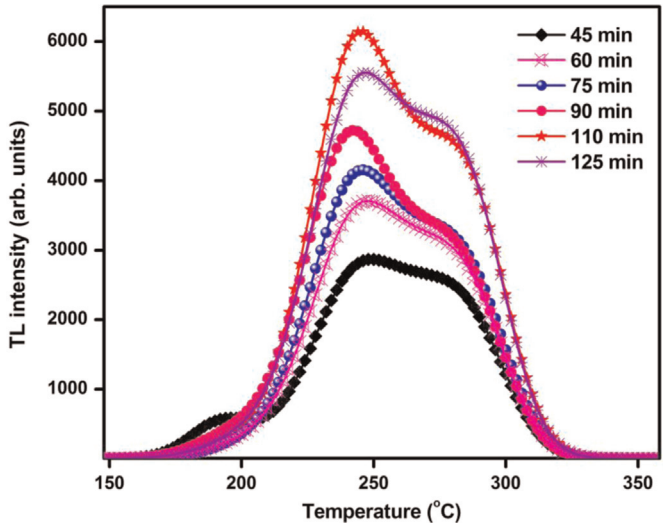

Fig. 8. TL glow curves of $LiNa_{3-x}P_2O_7:xTb^{3+}$ (x=9 mol%) phosphor as a function of UV exposure time.

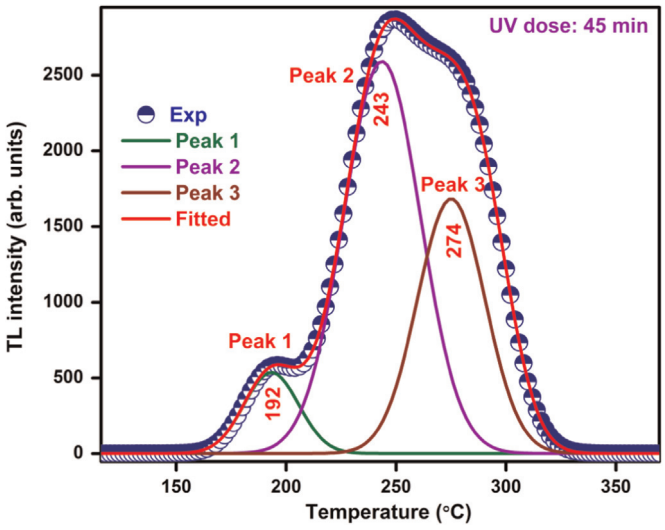

Fig. 9. A typical Gaussian fit of TL glow curve of $LiNa_{3-x}P_2O_7:xTb^{3+}$ (x=9 mol%), exposed to UV dose for 45 min.

the TL intensity is increased with the raise of UV exposure time up to 110 min and thereby decreased further increase in exposure time. This phenomenon could be explained on the basis of Horowitz's TIM (track interaction model) [39]. According to this model, at low exposure time, the recombination of various trapping/luminescent centers (TCs/LCs) encounters within the tracks. In the intermediate region, the electron will escape from the tracks due to the non-radiative centers. Therefore, TL intensity increases linearly with the irradiation time and is proportional to the UV dose (the exposure time). At higher dosage levels, the electrons leaving the track to the neighboring tracks will increases the recombination, because of the distance between the neighboring tracks are very less, hence; resulting the decrease in TL intensity. In the current case, the TL intensity increases with UV exposure time, since the number of particles irradiated increases with exposure time [40]. It is well known that the TL glow curve gives information regarding kinetic parameters, traps of material as well as mechanism responsible for the TL emission in material. The activation energy (E_γ) and the frequency factor of isolated peaks were evaluated using the Chen's peak shape method [41]. The activation energy (E_γ) can be estimated using the following equation:

$$E_\gamma = c_\gamma\left(\frac{kT_m^2}{\gamma}\right) - b_\gamma(2kT_m) \tag{6}$$

where, γ stands for τ, δ and ω, and $\omega = T_2 - T_1$ and $\delta = T_2 - T_m$ is half width towards fall-off side of glow curve, $\tau = T_m - T_1$ is full width at half maximum of the glow curve, T_m is the peak temperature corresponding to maximum intensity and T_1 and T_2 are the temperatures on either side of T_m corresponding to half of maximum intensity. The values of c_γ and b_γ are summarized as $c_\tau = 1.510 + 3.0$ $(\mu - \Delta)$, $b_\tau = 1.58 + 4.2$ $(\mu - \Delta)$, $c_\delta = 0.976 + 7.3$ $(\mu - \Delta)$, $b_\delta = 0$, $c_\omega = 2.52 + 10.2$ $(\mu - \Delta)$ and $b_\omega = 1$, where $\Delta = 0.42$ and 0.52 for first and second order TL peaks, respectively. The frequency factors could be determined by the formula

$$s = \frac{\beta E}{kT_m^2}\left(\frac{e^{\frac{E}{kT_m}}}{1 + \frac{(b-1)2kT_m}{E}}\right) \tag{7}$$

The deconvoluted TL graphs of $LiNa_{3-x}P_2O_7:xTb^{3+}$ (x=9 mol%) exposed to UV dose for 45 min is shown in Fig. 9. The order of kinetics (μ_g) was calculated for all peaks, indicating that that the phosphors obey the second-order kinetics [42,43]. The kinetics, trap parameters and frequency factors of $LiNa_{3-x}P_2O_7:xTb^{3+}$ (x=9 mol%) phosphors are calculated and summarized in Table 2. From the TL studies, it could be concluded that the phosphate based phosphor, $LiNa_{3-x}P_2O_7:xTb^{3+}$ (x=9 mol%) has linear response over a particular range of exposure and good sensitivity, which may be useful for its applications in radiation dosimetry.

Table 2
Kinetic parameters of $LiNa_{3-x}P_2O_7:xTb^{3+}$($x$=9 mol%) phosphor exposed to UV dose for 45 min.

UV dose (min)	Peak	T_m (°C)	b (μ_g)	E (eV)				s (s^{-1})
				E_τ	E_δ	E_ω	E_{avg}	
45	1	192	2 (0.52)	2.234	2.090	2.172	2.165	1.0E+25
	2	243	2 (0.49)	1.703	1.684	1.705	1.697	8.0E+17
	3	274	2 (0.50)	2.321	2.230	2.290	2.281	2.7E+22
60	1	216	2 (0.52)	1.452	1.408	1.436	1.432	1.1E+16
	2	243	2 (0.48)	1.753	1.740	1.760	1.751	2.8E+18
	3	287	2 (0.48)	2.526	2.443	2.504	2.491	7.2E+23
75	1	222	2 (0.50)	1.255	1.264	1.267	1.262	1.2E+14
	2	242	2 (0.50)	1.931	1.873	1.914	1.906	1.1E+20
	3	279	2 (0.50)	1.903	1.858	1.892	1.884	3.3E+18
90	1	239	2 (0.48)	2.097	2.042	2.085	2.075	7.2E+21
	2	272	2 (0.49)	1.909	1.879	1.907	1.898	7.7E+18
110	1	245	2 (0.48)	1.525	1.532	1.539	1.532	1.5E+16
	2	284	2 (0.50)	2.274	2.191	2.247	2.237	4.3E+21
125	1	239	2 (0.49)	1.975	1.930	1.967	1.957	4.7E+20
	2	285	2 (0.49)	2.113	2.067	2.105	2.095	1.9E+20

4. Conclusion

In conclusion, the green emitting alkaline based phosphate phosphor $LiNa_3P_2O_7:Tb^{3+}$ have been synthesized by the solid state reaction method. The phosphors were crystallized in orthorhombic structure. The pyrophosphate groups were confirmed by FTIR. Emission characteristics of the phosphors show more intense emission in green region (545 nm) due to $^5D_4 \rightarrow {}^7F_5$ transition under excitation (378 nm) of near-UV. The CIE color coordinates were located in the green region. From spectroscopic investigation, it shows that the $LiNa_{3-x}P_2O_7:xTb^{3+}$ (x=9 mol%) phosphor may be potential candidate for green emitting light under NUV excitation. TL glow curve of $LiNa_{3-x}P_2O_7:xTb^{3+}$ (x=9 mol%) indicates that it obeys second order-kinetics and it responds linearly to increasing UV exposure time. The mean trap depth (E) and frequency factor (s) of the phosphors were calculated by using Chen's peak shape method.

Acknowledgments

One of the authors, B. Deva Prasad Raju is highly grateful to DST-SERB, Department of Science and Technology, Government of India, India, for providing financial assistance in the form of Fast track research project (Young Scientist Award); vide Reference number, DST-SR/FTP/PS-198/2012; dated-14-02-2014.

References

[1] C.C. Lin, Z.R. Xiao, G.Y. Guo, T.S. Chan, R.S. Liu, J. Am. Chem. Soc. 132 (2010) 3020–3028.
[2] G. Li, D. Geng, M. Shang, Y. Zhang, C. Peng, Z. Cheng, J. Lin, J. Phys. Chem. C 115 (2011) 21882–21892.
[3] G. Ju, Y. Hu, L. Chen, X. Wang, Z. Mu, H. Wu, F. Kang, Opt. Laser Technol. 44 (2012) 39–42.
[4] S. Nakamura, G. Fasol, The Blue Laser Diode, Springer, Berlin, 1996.
[5] G. Li, D. Geng, M. Shang, C. Peng, Z. Cheng, J. Lin, J. Mater. Chem. 21 (2011) 13334–13344.
[6] M. Shang, C. Li, J. Lin, Chem. Soc. Rev. 43 (2014) 1372–1386.
[7] S. Som, A.K. Kunti, V. Kumar, V. Kumar, S. Dutta, M. Chowdhury, S.K. Sharma, J. J. Terblans, H.C. Swart, J. Appl. Phys. 115 (2014) 193101–193114.
[8] S. Choi, J. Yun, H.K. Jung, Mater. Lett. 75 (2012) 186–188.
[9] X. He, M. Guan, N. Lian, J. Sun, T. Shang, J. Alloy. Compd. 492 (2010) 452–455.
[10] F. Daniels, C.A. Boyd, D.F. Saunders, Science 117 (1953) 343.
[11] T. Aydın, H. Demirtas, S. Aydin, Radiat. Meas. 58 (2013) 24–32.
[12] M.T. Jose, S.R. Anishia, O. Annalakshmi, V. Ramasamy, Radiat. Meas. 46 (2011) 1026–1032.
[13] Z.J. Zhang, J.L. Yuan, C.J. Duan, D.B. Xiong, H.H. Chen, J.T. Zhao, G.B. Zhang, C. S. Shi, J. Appl. Phys. 102 (2007) 093514–093517.
[14] G. Li, X. Xu, C. Peng, M. Shang, D. Geng, Z. Cheng, J. Chen, J. Lin, Opt. Express 19 (2011) 16423–16431.
[15] G.R. Dillip, S.J. Dhoble, L. Manoj, C.M. Reddy, B.D.P. Raju, J. Lumin. 132 (2012) 3072–3076.
[16] D. Deng, H. Yu, Y. Li, Y. Hua, G. Jia, S. Zhao, H. Wang, L. Huang, Y. Li, C. Lia, S. Xu, J. Mater. Chem. C 1 (2013) 3194–3199.
[17] E. Song, W. Zhao, G. Zhou, X. Dou, C. Yi, M. Zhou, J. Rare Earths 29 (2011) 440–443.
[18] J. Zhou, Z. Xia, H. You, K. Shen, M. Yang, L. Liao, J. Lumin. 135 (2013) 20–25.
[19] G. Li, C. Li, C. Zhang, Z. Cheng, Z. Quan, C. Peng, J. Lin, J. Mater. Chem. 19 (2009) 8936–8943.
[20] T. Jiang, X. Yu, X. Xu, H. Yu, D. Zhou, J. Qiu, Mater. Res. Bull. 51 (2014) 80–84.
[21] V. Kumar, S. Som, V. Kumar, V. Kumar, O.M. Ntwaeaborwa, E. Coetsee, H. C. Swart, Chem. Eng. J. 255 (2014) 541–552.
[22] S. Chen, Y. Wang, J. Zhang, L. Zhao, Q. Wang, L. Han, J. Lumin. 150 (2014) 46–49.
[23] G. Li, Z. Hou, C. Peng, W. Wang, Z. Cheng, C. Li, H. Lian, J. Lin, Adv. Funct. Mater. 20 (2010) 3446–3456.
[24] A.A. Ansari, A.K. Parchur, M. Alam, A. Azzeer, Mater. Chem. Phys. 147 (2014) 715–721.
[25] Y. Shi, Y. Wang, S. Pan, Z. Yang, X. Dong, H. Wu, M. Zhang, J. Cao, Z. Zhou, J. Solid State Chem. 197 (2013) 128–133.
[26] A. Zaafouri, M. Megdiche, M. Gargouri, J. Alloy. Compd. 584 (2014) 152–158.
[27] R.D. Shannon, Acta Crystallogr. A 32 (1976) 751.
[28] Y.Q. Jia, J. Solid State Chem. 95 (1991) 184.
[29] G.R. Dillip, P.M. Kumar, B.D.P. Raju, S.J. Dhoble, J. Lumin. 134 (2013) 333–338.
[30] A.M. Pires, M.R. Davolos, Chem. Mater. 13 (2001) 21–27.
[31] D.E. Corbridge, M. Grayson, G. Wiley, Griffith (Eds.), Topics in Phosphorus Chemistry, New York, 1966.
[32] G.R. Dillip, B.D.P. Raju, J. Alloy. Compd. 540 (2012) 67–74.
[33] Z. Wang, Z. Yang, P. Li, Q. Guo, Y. Yang, J. Rare Earths 28 (2010) 30–34.
[34] G. Blasse, B.C. Grabmaier, Luminescent Materials, Springer, Berlin, 1994.
[35] D.L. Dexter, J. Chem. Phys. 21 (1953) 836–844.
[36] L.G. VanUitert, J. Electrochem. Soc. 114 (1967) 1048–1056.
[37] S. Som, P. Mitra, V. Kumar, V. Kumar, J.J. Terblans, H.C. Swart, S.K. Sharma, Dalton Trans. 43 (2014) 9860–9871.
[38] Q. Liu, Y. Liu, Z. Yang, X. Li, Y. Han, Spectrochim. Acta A 87 (2012) 190–193.
[39] Y.S. Horowitz, O. Avila, M. Rodriguez-Villafuerte, Nucl. Instrum. Methods Phys. Res. B 184 (2001) 85–112.
[40] Y.S. Horowitz, M. Rosenkrantz, S. Mahajana, D. Yosian, J. Phys. D: Appl. Phys. 9 (1995) 205–211.
[41] R. Chen, J. Electrochem. Soc. 116 (1969) 1254–1257.
[42] G. Rani, P.D. Sahare, Nucl. Instrum. Methods Phys. Res. B 311 (2013) 71–77.
[43] K.V. Dabre, S.J. Dhoble, Adv. Mater. Lett. 4 (2013) 921–926.